Thermomechanical ablation under plasmonic field excited by ultrashort laser pulse. Part II

IOP Conf. Series: Journal of Physics: Conf. Series **1092** (2018) 012052 doi:10.1088/1742-6596/1092/1/012052

Thermomechanical ablation under plasmonic field excited by ultrashort laser pulse. Part II

A.I. Ignatov[1,2,3], **V.V. Zhakhovsky**[1,4], **A.M. Merzlikin**[1,2,3], **and N.A. Inogamov**[4,1]

[1] Dukhov Research Institute of Automatics, 22 ul. Sushchevskaya, Moscow 127055, Russia
[2] Moscow Institute of Physics and Technology, 9 Institutskiy per., Dolgoprudny, Moscow Region, 141700, Russia
[3] Institute for Theoretical and Applied Electromagnetics of the Russian Academy of Sciences, 13 Izhorskaya ul., Moscow 125412, Russia
[4] Landau Institute for Theoretical Physics of the Russian Academy of Sciences, 1a prosp. Akademika Semenova, Chernogolovka, Moscow Region 142432, Russia

E-mail: nailinogamov@gmail.com

Abstract. Electrodynamic modeling of running SPP (surface plasmon-polaritons) and interference of the SPP wave with the beam 2 are presented in Part I of our work. Standing wave with alternating hot (antinodes) and cold (nodes) intervals appears thank to the interference. Electrodynamic simulations provide distribution of absorbed energy along the hot and cold intervals, which is utilized in this Part II. Here we discuss how can the ultrafast spatially alternating heating be imprinted into the periodic shape perturbations of a thin film atop a substrate. The Kretschmann's configuration (Kc) and additional (relative to Kc) laser beam #2 for periodic ripples of the film is used.

1. Introduction. Popular techniques of surface nanomodification utilize the ultrafast lasers, e.g. see [1, 2, 3]. Single or multiple laser actions with a number of shots $N > 1$ can be used to fabricate surface nanostructures. In the present work we consider optical lasers and single pulses; x-ray lasers need special analysis. Difference between single and multiple actions in the plane $(N, F_{\rm abs})$ is discussed in [4], see figure 11 in this Ref. Hereinafter $F_{\rm abs}$ is laser energy absorbed or dissipated in a target. In addition, structures formed by laser heating of a metal target through transparent liquid (laser ablation in liquid) have been studied. Different structures appear in the cases with large $R_{\rm L} \gg \lambda$ and small $R_{\rm L} \sim \lambda$ (tight focusing) illuminated spots; here $R_{\rm L}$ is the radius of surface spot illuminated by a beam with a Gaussian spatial distribution of laser intensity, the wavelength λ is $\sim \mu$m for the visible light.

Random nanostructures are formed in the case of large spots [4, 5, 6, 7]. Because we exclude from consideration the case of multiple illuminations of the same spot by $N > 1$ shorts, the LIPSS (laser induced periodic surface structures) are not studied here. The minimal spatial scales of the random surface nanostructures are determined by the surface tension, but not by the light wavelength λ. Diffraction-limited small spots are also used for nanostructuring, but the corresponding structures are very different from those which appear in large spots. Tight focusing produces individual structures – one per a small spot, and those structures are usually used as elements of a large array [3, 8, 9]. There are two methods of manufacturing the array of nanostructures. One of them uses frequent repetitions of shots simultaneously with shifting

of surface. Thus every new shot comes to a fresh (previously unirradiated) spot, e.g. see figure 1 in [9]. In the second method a laser ray is split into a few subrays which interfere with each other thus producing simultaneously an array of small illuminated spots on the surface [3].

Above we list known methods of nanomodification of metal surface. The new method proposed here is based on a fine spatial redistribution of dissipated energy governed by surface plasmons. The scheme of the method of nanostructuring is given in figure 1 of the Part I.

2. Splitting the time scales. The problem stated above is too complicated to be numerically solved from its beginning to the end, because the development of a multi-physics computation code requires great efforts. To follow formation of nanostructures at a surface of metal film under the action of electromagnetic (EM) field, the electrodynamic (ED) and thermomechanical processes, both, have to be taken into account in one straight-through code. At the input of such code the target and a laser pulse characteristics should be given. At the output we expect to get a spatially deformed film which has been subjected to heating, melting, and shifting before freezing and forming the final nanostructure. Developing of such multi-physics code is work for future.

We solve the problem by splitting into three time scales. There are three codes and three stages at which the different processes corresponding to these three time scales are simulated. The output of the first code is the input for the second one, while the second output is the input for the third code.

The deformed surface is created from initially smooth plane film. We use a gold film with the thickness $d_\mathrm{f} = 80$ nm, see Part I, deposited atop a dielectric prism. The first time scale ~ 1 ps is defined by duration of a laser pulse τ_L and duration needed for homogeneous heating the film through its thickness d_f; spread of dissipated heat along a spatial period of a plasmonic wave ~ 0.7 μm takes much longer times ($\sim$ nanoseconds) and relates to the third stage. We use electrodynamic (ED) code to describe excitation of plasmonic wave by the first laser beam, its interference with the second laser beam, formation of a standing wave, and dissipation in the standing wave, see figure 1 in Part I. The first stage is short relatively to the acoustic time $t_\mathrm{s} = d_\mathrm{f}/c_\mathrm{s} = 27$ ps, where the sound speed $c_\mathrm{s} = 3.1$ km/s. Mechanical interaction of a fast heated film with substrate lasts $\sim t_\mathrm{s}$. This is the second stage which we solve using the second code: the one-dimensional (1D) two-temperature (2T) hydrodynamic code (2T-HD) [8]. Comparing the first and the second time scales we conclude that we can employ the ED code neglecting appearance of a gap between a film and substrate. The ED code gives distribution of thermal heating along the film; this distribution (obtained in Part I) serves as a starting state for thermomechanical simulations of the second and the third stages (these two stages are described in this Part II).

Only later at the long stage 3 a slow thermal cross-flow between the places where the hot antinodes and the cold nodes of the standing wave were located becomes significant in the energy balance. Due to thermal outflow outside the region occupied by the spot 2 of the laser beam 2 shown in figures in Part I leads to final freezing of the nanostructures. Freezing time should be less than tens nanoseconds to keep structure shapes formed by the ED imprint when the liquid film can move. If a longer time is required for cooling the structure will be smoothed out by capillary effects before freezing. Cooling rates impose strong limitation on the lateral size of the structured spot at the surface which should be less than few tens microns or we have to design alternative scheme of cooling with the usage of substrate with higher thermal conduction.

3. Thermomechanical response to plasmonic heating. For the stage 3 we employ the MD-MC code combining the molecular dynamics (MD) and Monte-Carlo (MC) methods [8]. Monte-Carlo subroutine allows to include electron heat conduction which is high in metal. Combined program follows material motion, melting, fast cooling and recrystallization. It should be emphasized that the non-equilibrium recrystallization with strong overcooling of liquid below melting temperature takes place at our spatiotemporal scales.

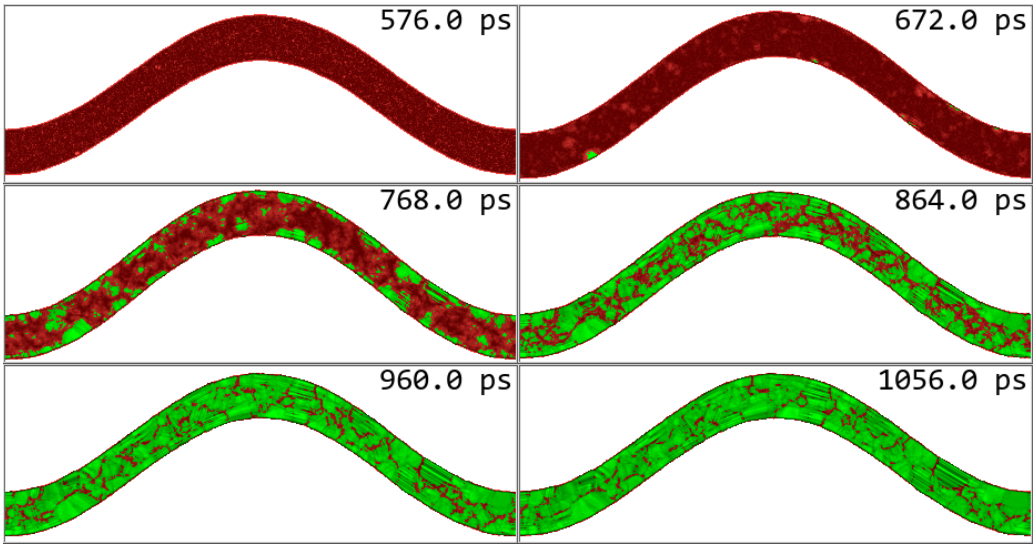

Figure 1. MD-MC simulated development of the SPP rippling. If the film remains in a liquid state, the height of sinusoidal-like perturbation will decrease later in time. Here inertia, surface tension, and the cooling rate are so that solidification proceeds at the stage of capillary stopping. The red color refer to the liquid phase, green – the solid state. Crystallization begins in strongly overcooled liquid gold, and the tiny crystallites of solid phase form gradually at the surface and in the bulk of gold.

In 2T-HD calculations we use the previously established (a) heat conduction coefficient valid in 2T and 1T states [10]; (b) electron-ion coupling parameter [10]; and (c) equation of state of gold [11], which is also valid for 2T and 1T states. 2T effects are significant because the duration of two-temperature relaxation 7–10 ps is comparable to acoustic time scale t_s for gold. The nonequilibrium 2T gold is softer than 1T one at the same density and total internal energy. Because in the 2T state a part of pressure is produced by excited electrons which have 2–3 times lower Gruneisen parameter [11]. This circumstance appreciably decreases expansion velocities at the same absorbed energy in comparison with the hypothetical case when gold always belongs to 1T state after absorption of plasmonic energy. Let's mention that equation of state used in the 2T-HD code describes well the first order phase transitions, melting and crystallization, which are important for our problem.

We use the 2T-HD code to determine the distributions of the temperature $T(x)$ and velocity $v(x)$ along a film, which are the output functions from the stage 2. To calculate those distributions the function $F_{\mathrm{abs}}(x)$ of dissipated fluence, which is the output function from the ED stage 1 and the input function for the stage 2 (2T-HD), is used.

Dynamics of one wavelength perturbation in a film under the periodic lateral boundary conditions was considered in a series of MD-MC simulations. Typical results are presented in figure 1. It shows evolution of a film after melting, separation from substrate, deformation under surface tension action, and solidification. Initial thickness of the gold film is 20 nm in our MD-MC simulations. Horizontal length (i.e. in x direction) of the rectangular box is $L = 200$ nm. Thickness of the simulation box in the z direction (perpendicular to the plane of figure 1) is 12 nm. Temperature of gold after fast melting is 1800 K. In this run we neglect the temperature difference along a simulation box because the main thermal process is not equilibration of temperature along a period of a SPP wave but cooling due to transfer of thermal energy outwards the hot spot 2, see Part I. In simulations we use the accurate EAM (embedded atom model) interatomic potential for gold [12] developed using the stress-matching

method with the stress-strain curves obtained by DFT (density functional theory). This EAM potential gives the melting temperature of 1330 K close to the experimental melting point of 1337 K for gold.

Initially the velocity distribution $v(x) = v_0 \cos(2\pi x/L)$ with $v_0 = 50$ m/s is imposed in the run presented in figure 1. 2T-HD simulations show that for our range of dissipated energies the velocities of a film after separation are of the order of a few tens of m/s [8]. Capillary scale of speed is $v_{\rm cap} = 2\sqrt{\sigma/(\rho d_{\rm f})}$, where σ is the surface tension, ρ is the density of gold. This speed is 56 m/s for the film with $d_{\rm f} = 80$ nm and $\sigma = 1200$ erg/cm^2. In our MD-MC simulations $d_{\rm f} = 20$ nm and EAM potential has $\sigma \approx 600$ erg/cm^2. Then $v_{\rm cap} = 79$ m/s. MD-MC simulations show that to decelerate a film effectively and to prevent jetting the surface tension should be sufficiently strong to resist inertia. Then the dimensionless capillary normalized velocity $2v_0/v_{\rm cap}$ should be of the order of 1 or less [8]. In the run given in figure 1 the evolution of one SPP period of a film is followed in the coordinate system connected with a center of mass of this period. Momentum of the period is equal to zero in this system. This period moves outward in other coordinate system connected with the bulk of substrate . This corresponds to the few central bumps in the chain of bumps or periods of the SPP wave train covering the spot 2, see paper I. The bumps outside this central interval remains intact with substrate.

There are different situations depending on the dimensionless capillary normalized velocity and the rate of cooling, see [8]. In simulations we use the Langevin thermostat to reach the goal temperature 600 K with the characteristic cooling time 400 ps. The thermostat acts only on the z-component of atom velocity which is perpendicular to the plane of motion. Thus the thermostat does not decelerate motion in the x, y plane shown in figure 1. The thermostat provides approximately homogeneous cooling of gold inside the SPP period due to thermal energy transport outwards from the hot spot 2 which includes a train of the standing SPP wavelengths, see Part I.

The panels in figure 1 show evolution of phase states during cooling and freezing the film. Due to fast cooling the molten gold goes into a deeply supercooled state. Only at time of 590 ps an appreciable growth of nuclei of solid phase begins at temperatures ≈ 870 K, which is much below the equilibrium melting temperature of 1330 K for simulated gold. Nucleation starts like a explosive process driven by homogeneous appearance of multiple seeds of solid state everywhere in a film volume, because metastable liquid gold reaches a significant supercooling degree. Such homogeneous volume solidification takes few hundreds picoseconds to finally freeze gold and stop motion of the film.

Acknowledgements
Work of NAI and VVZ was supported by the RSF grant 14-19-01599.

References

[1] Domke M, Rapp S, Schmidt M and Huber H P 2012 *Opt. Express* **20** 10330–10338
[2] Ivanov D S, Kuznetsov A I, Lipp V P, Rethfeld B, Chichkov B N, Garcia M E and Schulz W 2013 *Applied Physics A* **111** 675–687
[3] Nakata Y, Miyanaga N, Momoo K and Hiromoto T 2013 *Appl. Surf. Sci.* **274** 27–32
[4] Inogamov N, Zhakhovsky V, Ashitkov S, et al 2015 *Engineering Failure Analysis* **47** 328 – 337
[5] Wu C and Zhigilei L V 2016 *J. Phys. Chem. C* **120** 4438–4447
[6] Zhakhovskii V V, Inogamov N A and Nishihara K 2008 *JETP Letters* **87** 423–427
[7] Fang R, Vorobyev A and Guo C 2017 *Light: Sci. Appl.* **6** e16256
[8] Wang X W, Kuchmizhak A A, Li X, Juodkazis S, Vitrik O B, Kulchin Y N, Zhakhovsky V V, Danilov P A, Ionin A A, Kudryashov S I, Rudenko A A and Inogamov N A 2017 *Phys. Rev. Appl.* **8**(4) 044016
[9] Kuchmizhak A, Vitrik O, Kulchin Y, et al 2016 *Nanoscale* **8**(24) 12352–12361
[10] Petrov Y, Inogamov N and Migdal K 2013 *JETP Lett.* **97** 20–27
[11] Petrov Y V, Migdal K P, Inogamov N A and Zhakhovsky V V 2015 *Applied Physics B* **119** 401–411
[12] Zhakhovskii V, Inogamov N, Petrov Y, Ashitkov S and Nishihara K 2009 *Appl. Surf. Sci.* **255** 9592 – 9596